Facile approach to generating polymeric nanoarrays containing populations of nanoparticles

Leonel Marques[1], Xinyong Chen[2], Clive J. Roberts[2], Matthew Clark[1], Jonathan W. Aylott[2]

[1]*Applied Optics Group, Electrical and Electronic Engineering, University of Nottingham, University Park, Nottingham NG7 2RD, UK*
[2]*School of Pharmacy, University of Nottingham, University Park, Nottingham NG7 2RD, UK*
E-mail: leonel.marques@nottingham.ac.uk

Published in Micro & Nano Letters; Received on 30th January 2015; Accepted on 13th May 2015

The production of nanoarrays containing a population of entrapped, heterogeneous nanoparticles is reported. The nanoarray consists of a nanoporous film with pores of diameter 60–180 nm, formed from the phase separation of two immiscible polymers: polystyrene (PS) and polymethylmethacrylate coated onto glass or silicon wafer. Nanoparticles of PS (120 nm) and silica (90 nm) were deposited into the nanoporous films to generate the nanoarray containing a mixed population of nanoparticles.

1. Introduction: In this Letter, we demonstrate a facile, low-cost method for fabricating a nanoarray containing a heterogeneous population of nanoparticles. These arrays, when used in conjunction with previously developed nanosensor technology [1–3] have potential for application in biomedical sensing/diagnostics where multi-sensor surfaces or 'smart slides' could be developed. The arrays consist of a nanoporous polymer film loaded with nanoparticles which sit in holes in the nanoporous polymer film, akin to a nanoscale version of eggs in an eggbox. By including a mixed population of nanoparticles in the array it would be possible to incorporate a range of nanosensors, selective to different analytes, together in one sensing platform on a single glass slide. The nanoarray presented here offers the potential to increase the number of test spots used in current microarray technology [4] such that surfaces with a density of 1000 nanoparticles in an area of 100 μm^2 can be fabricated. The high density of nanoparticles sensors gives a potential increase in sensitivity and detection when measuring small samples.

Nanoarrays having each nanoparticle acting as a sensor could generate a high-throughput array for the detection of many analytes. Compared with the microarray technology, however, obtaining the readout from a nanoarray is challenging as reading the optical output from individual nanoparticles presents a problem because of the lateral spatial resolution being limited by the diffraction of light in optical microscopy. Nevertheless, the family of super-resolution optical imaging techniques such as photoactivated localisation microscopy [5], stochastic optical reconstruction microscopy [6], stimulated emission depletion microscopy [7] and structured illumination microscopy [8] are in continuous development and will make it possible to address single particles in a nanoarray. Previously reported nanoarrays have been fabricated using diverse nanolithographic techniques [9], examples are dip-pen nanolithography [10], electron beam lithography [11], focused ion-beam lithography [12], nanosphere lithography [13], as well as nanoimprint lithography [14]. In contrast to these 'top-down' techniques it is also possible to use 'bottom-up' approaches to generate patterned nanoscale areas. Nanoscale features can be generated using the self-assembly of diblocks copolymer thin films without the requirement for complex lithography techniques [15, 16]. In this Letter, we have exploited the self-assembling nature of two immiscible polymers [polystyrene (PS) and polymethylmethacrylate (PMMA)] to fabricate a nanoporous film on glass and silicon substrates. Further, we have used this nanoporous surface as a template to deposit nanoparticles in single nanoscale pores, thus creating the nanoarray. Fig. 1 is a schematic drawing outlining the main steps of the construction of the array.

2. Experimental details

2.1. Nanoporous polymer film formation: The silicon substrates and the glass coverslips were cleaned with 'piranha' solution (3:1 ratio of sulphuric acid and hydrogen peroxide (30%)) and then left to stand in the solution for 45 min. The substrates were washed thoroughly with deionised water and dried out with nitrogen. PS ($M_w = 13$ K) and PMMA ($M_w = 10$ K) were used without any further purification and modification. The polymers were dissolved in toluene in the weight ratio 5 wt% PS:PMMA (75:25) and spun-cast at 3000 rpm as a thin film on a clean silicon wafer

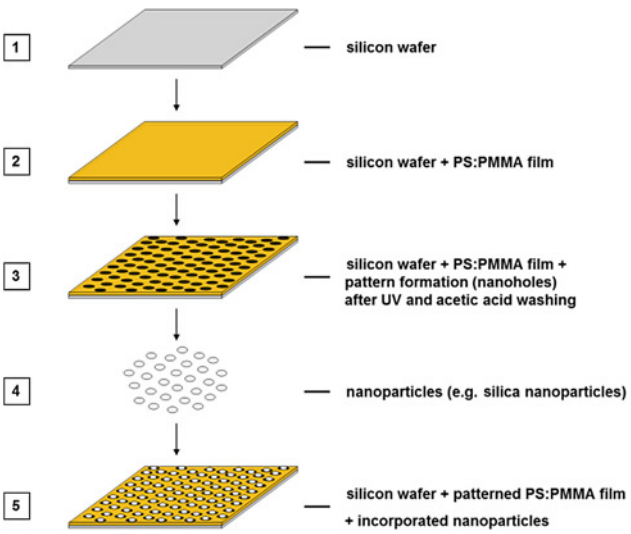

Figure 1 *Schematic diagram of the several steps for the nanoarray formation*
1. A clean piece of silicon wafer is used as the main substrate (note: a glass substrate was also used); 2. A layer of a polymeric solution made of PS and PMMA with a specific ratio is spin-coated onto the substrate; 3. The polymeric film is treated to generate a patterned surface of nanoholes along the film; 4. Nanoparticles are fabricated; 5. Final assembly is performed having the nanoparticles entrapped inside the nanoholes of the nanoporous film

doi: 10.1049/mnl.2015.0041

or glass coverslip. The thin films were annealed under vacuum for 24 h in an oven at 125°C. The annealed film was placed under an ultraviolet (UV) lamp (254 nm) for 30 min and washed with glacial acetic acid (2 ml) followed with an extensive deionised water wash. The resultant nanoporous film was dried out with nitrogen.

2.2. Nanoparticles preparation: The PS beads with an average size of 100 ± 15 nm were used as purchased (from Sigma Aldrich, UK). The silica nanoparticles (SiNPs) were prepared via a modified Stober synthesis method [17]. A clean glass reaction vessel containing 16.75 ml of pure ethanol and 1.28 ml of ammonium hydroxide (28.8%) was prepared. The solvents were mixed for 20 min and 0.5 ml of tetraethyl orthosilicate was added. The solution was stirred for 24 h under an Argon flux and centrifuged at 12 000 rpm for 30 min to collect the nanoparticles. The nanoparticles were further washed twice with deionised water and once with ethanol by centrifugation at 12 000 rpm to remove the unreacted chemicals. The remaining pellet was resuspended in water and filtered using a 0.02 mm Anodisc 25 to recover the dried nanoparticles. The SiNPs had an average size of 80 ± 10 nm as determined by atomic force microscopy (AFM) and by dynamic light scattering with a Viscotek 802 (Malvern Instruments Ltd, UK) characterisation.

2.3. Incorporation of the nanoparticles on the nanoporous polymer film: A 0.75 ml mixture of 0.4 mg/ml of each nanoparticle solution, PS and SiNPs, was mixed to a final volume of 1.5 ml (50:50 volume ratio) and placed in contact with the polymeric film positioned at a 45° angle and left at 60°C in an oven until the remaining solvent was evaporated.

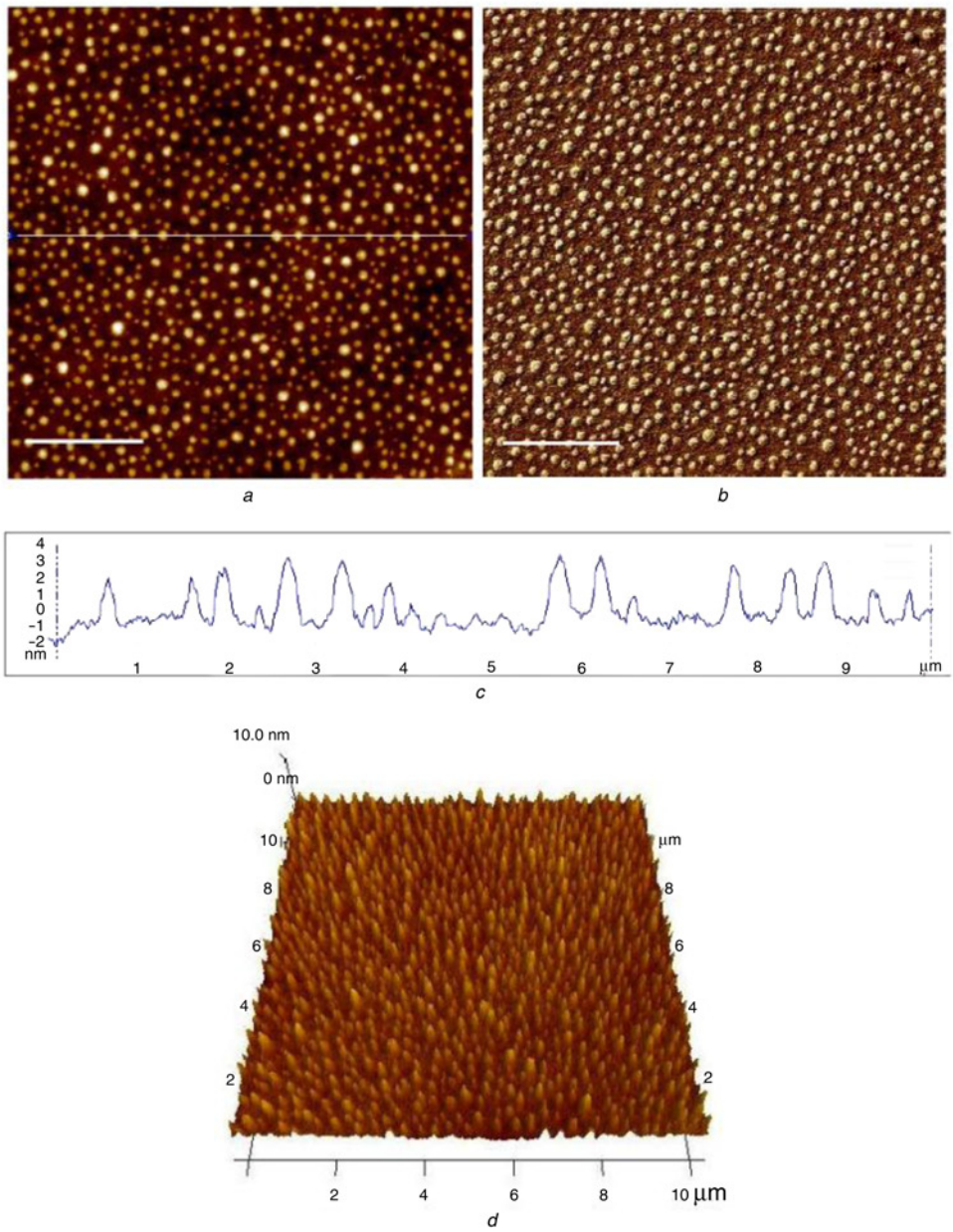

Figure 2 *TM-AFM images of the self-assembled nanostructured PS:PMMA film with PMMA protrusions surfacing from the PS main matrix*
a Height
b Phase
c Section
d Three-dimensional
Scale bar 2.5 mm

2.4. Characterisation of the nanoporous film with and without heterogenous nanoparticles: AFM measurements were performed using a multimode AFM with a Nanoscope V controller and Harmonix software (Veeco, Santa Barbara, CA, USA). TAP300 probes were used for tapping mode (TM)-AFM measurement and HMX probes (HMXTM) for harmonix measurement (both probers were from Veeco, Santa Barbara, CA, USA). The HMXTM cantilever has a typical spring constant of 4 N m^{-1}, a flexural resonant frequency of 54 kHz and a torsional resonant frequency of 1 MHz. The amplitude setpoint, drive amplitude and gains were adjusted during imaging. A calibration protocol as described in the Veeco Harmonix User Guide using the provided Standard Harmonix calibration sample [PS-LDPE (70:30)] was followed to calculate the detector sensitivity, cantilever spring constant, HarmoniX force sensitivity and other parameters to determine the correct quantity scales of the nanomechanical parameters. The AFM data was processed with the Scanning Probe Image Processor version 3.3.8 (SPIP) (Image Metrology, Horsholm, Denmark) and the Nanoscope V 7.30 (Veeco, Santa Barbara, CA, USA) softwares. The contact angle of the nanoporous film was determined with an optical contact angle meter CAM 200 (KSV Instruments Ltd, Finland).

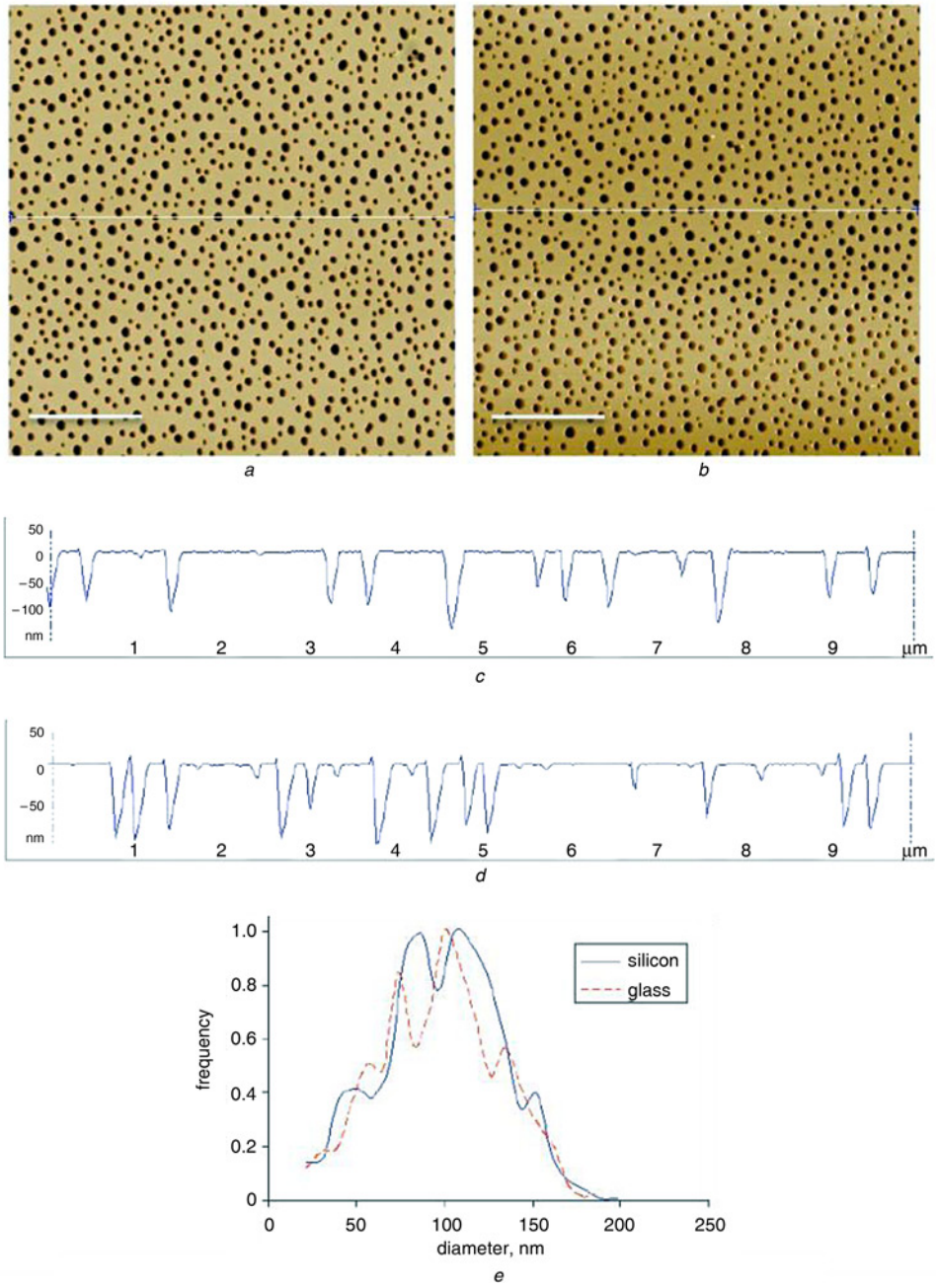

Figure 3 *TM-AFM height images of the produced nanoporous film after acid etching on silicon and glass*
a TM-AFM height image of the produced nanoporous film after acid etching on silicon wafer
b TM-AFM height image of the produced nanoporous film after acid etching on glass
Scale bar 2.5 µm
c Sectioning of the nanoporous film on silicon
d Sectioning of the nanoporous film on glass
e Histogram comparing the size of the nanoholes generated from the polymeric film when coated on silicon or glass
The nanoholes have an average ranging size (higher frequency) between 80 and 140 nm in both surfaces

doi: 10.1049/mnl.2015.0041

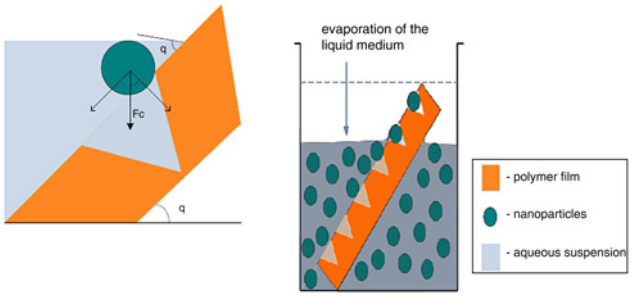

Figure 4 *Schematic drawing showing the liquid interface movement over the surface of the nanoporous film leading to the entrapment of nanoparticles*

3. Results and discussion: A PS and PMMA polymer solution mixed in a 5 wt% (75:25) ratio was spin-coated on two substrates: silicon and glass, forming a thin film (≤150 nm). The 75:25 ratio was initially selected for this work because of the size range of PMMA domains and its coverage obtained over the polymeric film. Other ratios like 85:15 and 80:20 lead to similar results for the size range of the PMMA domains; but with a variation of −5 and −2.5% of coverage per μm^2 compared with the ratio 75:25 (data not shown). This results in a pattern of PMMA circular domains emerging in the PS matrix. This can be seen in Fig. 2 that corresponds to step 2 in Fig. 1. The same film pattern morphology was observed on both substrates (data not shown). The phase imaging (Fig. 2*b*) also reveals a difference in the phase signal between the circular domains (PMMA) and the main matrix (PS). The difference in phase signal is due to the two different components in the sample composition. The sectioning and three-dimensional display enhances the architectural elevation of 4 nm from the PMMA domains above the main matrix (Figs. 2*c* and *d*). The film morphology is obtained since the PMMA domains raised first to the surface of the polymer solution during the phase separation. The freeze-in process during the spin-coating will happen faster for the PMMA domains because of the solvent used for the mixing of two polymers being toluene. PMMA is less soluble than PS in toluene, resulting in the PMMA domains being localised above the interface of the phase separation within the PS matrix. The minor phase (PMMA) along the major phase (PS) established a disperse phase morphology during the phase separation of the two immiscible polymers. The annealing temperature of 125°C was higher than the glass transition temperature for the PS to anneal and to avoid the 'dewetting' phenomenon of the film from the substrate surface.

The film was first exposed to UV light at a wavelength of 254 nm to decompose the annealed PMMA chains and to reinforce at the same time the annealing of the PS matrix along the film. By washing the film with glacial acetic acid, the PMMA domains

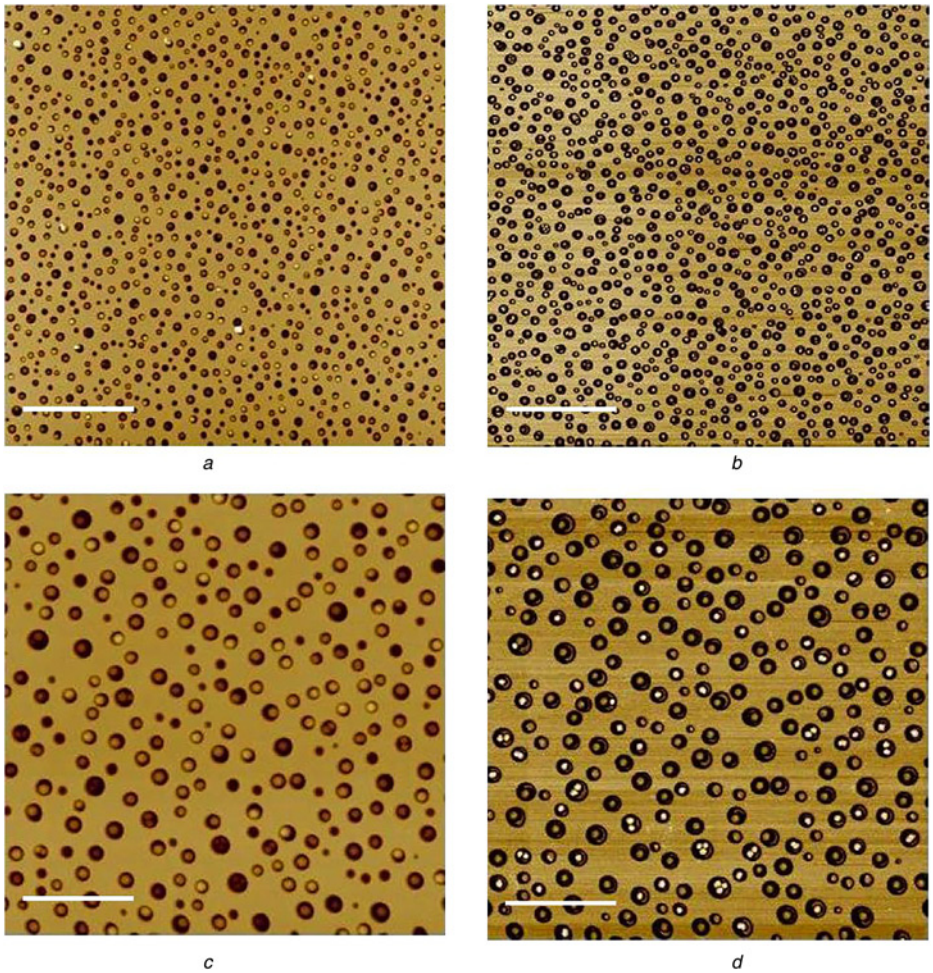

Figure 5 *TM-AFM images of the nanoporous film incorporating two different nanoparticles, PS beads and SiNPs, imaged from a silicon substrate*
a Height images of a non-zoomed area, scale bar 2.5 µm
b Phase images of a non-zoomed area, scale bar 2.5 µm
c Height images of a zoomed area, scale bar 1 µm
d Phase images of a zoomed area, scale bar 1 µm

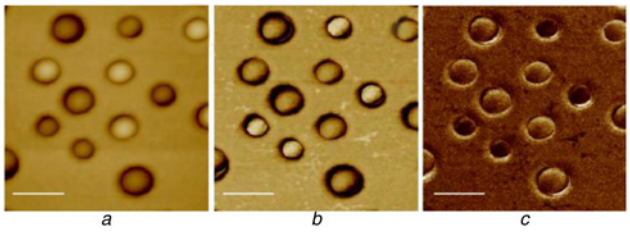

Figure 6 *TM-AFM images using a THC probe of the nanoporous film incorporating PS beads and SiNPs*
a Height
b Phase
c Adhesion
Scale bar 200 nm

were selectively removed. This generates a nanoporous PS film without any disruption of its original matrix. The process was repeated on silicon and glass substrates and revealed the same nanoporous structure (Figs. 3*a*–*d*). The process was found to be highly repeatable and produced a consistent and uniform structure over a wide area (> 1mm) confirmed by imaging randomly along the sample surface (data not shown). The patterned circular nanoholes distributed along the nanoporous film were analysed for their size profiling using the SPIP software. The results demonstrated that the mean diameter of the holes was ~100 nm for both substrates (Fig. 3*e*). It is thought that the larger holes are formed by aggregations of smaller holes during the film formation. The nanoporous template is generated and ready for the entrapment of the nanoparticles. It should be noted that the holes are not regular and uniformly distributed along the film since we did not use a diblock copolymer in this work. The use of diblock copolymers can generate well-organised, ordered cylindrical structures but the pore size range is limited to a maximum of 50 nm [18, 19].

The evaporation rate of the nanoparticles solution promotes a three-phase (vapours–suspension–substrate) contact line with the nanoporous film substrate [20, 21]. The three-phase line will move along the sample surface enabling the entrapment of nanoparticles into the nanoholes by the action of the capillary forces (F_c). The substrate is kept under a 45° angle position to ensure maximum entrapment of nanoparticles. The process is illustrated in Fig. 4. The matrix of the nanoporous film is made of PS that has a hydrophobic behaviour with a measured contact angle value of 72°. A ratio of water/ethanol (60:40) enabled the suspension to interact with the film surface. The ethanol decreased the contact angle value to near 40° approaching complete wetting of the film's surface. The ethanol molecules are going to be localised at the liquid/vapour interface rather than in the bulk of the solution [22]. If only water was used to suspend the nanoparticles, the entrapping rate will be <5%, the remaining nanoparticles agglomerated at the bottom of the film surface at the end of the evaporation process (data not shown). Once the deposition process is completed, the nanoporous film with the nanoparticles was characterised by AFM (Fig. 5). From the AFM imaging it is observed that all the nanoholes are filled with nanoparticles (Figs. 5*a* and *b*). The AFM height images fail in some cases to evidence that all the holes have nanoparticles; since the images rely on height measurement and some nanoparticles are located deeper inside the hole. These are observed when comparing height and phase images. The diameter size of the nanohole controls the number of nanoparticles to be incorporated into it. One nanoparticle will be entrapped if the diameter size is around 100–160 nm. More than one will be entrapped if the diameter size is larger than 160 nm.

The incorporation of two to three nanoparticles was observed. Nanoparticles organised themselves inside the nanohole into a geometrical arrangement related to the diameter size of the nanohole and the number of nanoparticles that can be allocated. The lateral immersion forces between the hydrophilic nanoparticles that take place in solution are also responsible for the allocation of more than one nanoparticle into the nanohole. As the liquid film becomes thinner during the displacement along the film, the liquid surface deformation increases, leading to a strong interparticle attraction [23], causing the observed self-assembly of the nanoparticles into the nanohole. The orientation of the nanoparticles inside the nanoholes is independent of the direction of the motion of the fluid interface during the evaporation, confirming an auto-arrangement during the entrapment (Figs. 5*c* and *d*).

The arrays were imaged using TM-AFM using a torsional harmonic cantilevers (THC) mode to probe adhesion and stiffness [24]. A typical image is shown in Fig. 6. This shows the normal height topography, phase and adhesion. The height image does not clearly identify the nanoparticles because the height depends on the depth that the particle sits in the pore and the size of the particle. The phase and adhesion images clearly differentiate between the PS and silica beads with PS beads giving values close to the PS film away from the pores. In the adhesion image (Fig. 6*c*), adhesion values for nanoparticles with a lighter colour (10.00 nN; assumed to be the PS beads) in comparison to the darker nanoparticles (3.52 nN; assumed to be the SiNPs) and PS film surface (9.32 nN) are obtained. The stiffness imaging (not shown) provides no useful contrast because the stiffness of both the PS and silica was outside of the measurable range of this AFM probe (spring constant = 4 N m^{-1} that is best suited for a surface hardness range between 0.05 and 3.0 GPa).

4. Conclusion: A simple process to develop a nanoporous film using a PS:PMMA blend mix solution was performed by the selective removal of the PMMA domains. The nanoporous film was used as a template to incorporate different nanoparticles. The film was formed into two different substrates, silicon and glass, with no pre-treatment and with the same reproducibility for extensive areas (1 cm). The angled deposition method was selective by entrapping nanoparticles inside the nanoholes by means of the actuation of capillary forces. A distinction between the PS beads and SiNPs was observed by looking at the phase and adhesion properties measured by the THC probe.

5. Acknowledgments: This work was supported by the School of Pharmacy and Applied Optics group from the University of Nottingham. Funding is acknowledged from the EPSRC.

6 References

[1] Webster A., Compton S.J., Aylott J.W.: 'Optical calcium sensors: development of a generic method for their introduction to cell using conjugated cell penetrating peptides', *Analyst*, 2005, **130**, pp. 163–170
[2] Liu J.B., Yang X.H., He X.X, *ET AL.*: 'Fluorescent nanoparticles for chemical and biological sensing', *Sci. China Chem.*, 2011, **54**, pp. 1157–1176
[3] Menon J.U., Jadela P., Tambe P., Vu K., Yuan B., Nguyen K.T.: 'Nanomaterials for photo-based diagnostic and therapeutic applications', *Theranostics*, 2013, **3**, pp. 152–166
[4] Wingren C., Borrebaeck C.A.K.: 'Progress in miniaturization of protein arrays: a step closer to high-density nanoarrays', *Drug Discov. Today*, 2007, **12**, pp. 813–819
[5] Hess S.T., Girirajan T.P.K., Mason M.D.: 'Ultra-high resolution imaging by fluorescence photoactivation localization microscopy', *Biophys. J.*, 2006, **91**, pp. 4258–4272
[6] Bates M., Huang B., Dempsey G.T., Zhuang X.: 'Multicolor super-resolution imaging with photo-switchable fluorescent probes', *Science*, 2007, **317**, pp. 1749–1753
[7] Willig K.I., Keller J., Bossi M., Hell S.W.: 'STED microscopy resolves nanoparticles assemblies', *New J. Phys.*, 2006, **8**, doi: 10.1088/1367-2630/8/6/106
[8] Gustafsson M.G.L.: 'Surpassing the lateral resolution limit by a factor of two using structured illumination microscopy', *J. Microsc.*, 2000, **198**, pp. 82–87

[9] Luttge R.: 'Massively parallel fabrication of repetitive nanostructures: nanolithography for nanoarrays', *J. Phys. D, Appl. Phys.*, 2009, **42**, doi: 10. 1088/0022-3727/42/12/123001
[10] Salaita K., Wang Y., Mirkin C.A.: 'Applications of dippen nanolithography', *Nat. Nanotechnol.*, 2007, **2**, pp. 145–155
[11] Palankar R., Medvedev N., Rong A., Delcea M.: 'Fabrication of quantum dot microarrays using electron beam lithography for applications in analyte sensing and cellular dynamics', *ACS Nano*, 2013, **7**, pp. 4617–4628
[12] Lu K., Zhao J.: 'Focused ion beam lithography and anodization combined nanopore patterning', *J. Nanosci. Nanotechnol.*, 2010, **10**, pp. 6760–6768
[13] Wei X.: 'Recent developments in the fabrication of ordered nanostructure arrays based on nanosphere lithography', *Recent Pat. Nanotechnol.*, 2010, **4**, pp. 194–204
[14] Hoff J.D., Cheng L.-J., Meyhofer E., Guo L.J., Hunt A.J.: 'Nanoscale protein patterning by imprint lithography', *Nano Lett.*, 2004, **4**, pp. 853–857
[15] Mai Y., Eisenberg A.: 'Self-assembly of block copolymers', *Chem. Soc. Rev.*, 2012, **41**, pp. 5969–5985
[16] Koo K., Ahn H., Kim S.-W., Ryu D.Y., Russell T.P.: 'Directed self-assembly of block copolymers in the extreme: guiding microdomains from the small to the large', *Soft Matter*, 2013, **9**, pp. 9059–9071
[17] Stober W., Fink A., Bohn E.J.: 'Controlled growth of monodisperse silica spheres in the micron size range', *Colloid Interface Sci.*, 1968, **26**, pp. 62–69
[18] Black C.T., Guarini K.W.: 'Structural evolution of cylindrical-phase diblock copolymer thin films', *J. Polym. Sci. A, Polym. Chem.*, 2004, **42**, pp. 1970–1975
[19] Han E., Stuen K., La Y., Nealy P., Gopalan P.: 'Effect of composition of substrate-modifying random copolymers on the orientation of symmetric and asymmetric diblock copolymer domains', *Macromolecules*, 2008, **41**, pp. 9090–9097
[20] Cui Y., Bjork M.T., Liddle J.A., Sonnichsen C., Boussert B., Alivisatos P.: 'Integration of colloidal nanocrystals into lithographically patterned devices', *Nano Lett.*, 2004, **4**, pp. 1093–1098
[21] Kuemin C., Huckstadt K.C., Lortscher E., *ET AL.*: 'Selective assembly of sub-micrometer polymer particles', *Adv. Mater.*, 2010, **22**, pp. 2804–2808
[22] Lundgren M., Allan N.L., Cosgrove T.: 'Wetting of water and water/ethanol droplets on a non-polar surface: a molecular dynamics study', *Langmuir*, 2002, **18**, pp. 10462–10466
[23] Kralchevsky P.A., Nagayama K.: 'Capillary interactions between particles bound to interfaces, liquid films and biomembranes', *Adv. Colloid Interface Sci.*, 2000, **85**, pp. 145–192
[24] Sahin O., Erina N.: 'High-resolution and large dynamic range nanomechanical mapping in tapping-mode atomic force microscopy', *Nanotechnology*, 2008, **19**, doi: 10. 1088/0957-4484/19/44/445717